Transparent Carbon Nanotube Network for Efficient Electrochemiluminescence Devices

Transparent Carbon Nanotube Network for Efficient Electrochemiluminescence Devices

Giovanni Valenti,*[a] Martina Zangheri,[a] Sandra E. Sansaloni,[a, b] Mara Mirasoli,[a] Alain Penicaud,[b] Aldo Roda,[a] and Francesco Paolucci[a, c]

Abstract: A carbon nanotube-based electrode that combines transparency and good conductivity was used for the first time to develop an electrochemiluminescence (ECL) device. It resulted in an excellent material for ECL applications thanks to the very favorable overpotential of amine oxidation that represents the rate-determining step for the signal generation in both research systems and commercial instrumentation. The use of carbon nanotubes resulted in a ten times higher emission efficiency compared with commercial transparent indium tin oxide (ITO) electrodes. Moreover, application of this material for proof-of-principle ECL imaging was demonstrated, in which micro-beads were used to mimic a real biological sample in order to prove the possibility of obtaining single cell visualization.

Introduction

Electrochemically generated chemiluminescence (ECL), also called electrochemiluminescence, is a luminescence induced by an electrochemical stimulus.[1] As an analytical technique, it possesses several advantages over photoluminescence and chemiluminescence, in particular for (bio)sensor applications.[2] The electrochemically induced method of generating a luminescence signal permits sensors with a low background signal and high sensitivity, good temporal and spatial resolution, robustness, versatility, and low cost.[3]

Key points for efficient generation of the signal are the electrode behavior and surface material. In fact, a high potential, which typically ranges between 0.8 and 1.2 V, needs to be applied to generate emission and this may induce a modification of the electrode–solution interface.[4] For example, when such a potential is applied to a platinum electrode, one of the most used electrode materials in ECL, a thin layer of platinum oxide is generated at the electrode interface, dramatically affecting the kinetics and the efficiency of the signal generation.[5]

Microfluidic chips are attracting significant attention in the diagnostic and life science fields as they provide low sample and reagents consumption, short assay times, high sensitivity, and the possibility for automation and integration of several analytical steps into one device. Owing to its positive features, ECL is very well suited for microfluidic chip applications and particularly attractive is the possibility of integrated devices in which the ECL photon emission is obtained in close proximity to the photon detector to improve detectability and device compactness.[6] For this purpose, transparent electrode materials are sought to enable integration of the photosensing element into the same platform as that bearing the electrodes in the ECL cell.[7]

Devices that combine optical transparency and good electrical conductivity are in general very interesting for analytical applications.[8] Some of the typical transparent electrode materials used for biosensor applications are metal oxides, for example, indium tin oxide (ITO). However, ITO usually exhibit sluggish kinetics for the electrochemical reactions involved in the ECL generation process.[9] Most of the nanostructured platforms developed until now have been based on quantum dots,[10] nanoparticles,[11] graphene,[12] or carbon nanotubes[9] and were applied to detect large families of important analytes, such as tumor markers, for DNA analysis, or biological warfare agents.[13] Carbon-based nanomaterials, and in particular carbon nanotubes (CNTs), play a pivotal role in this field owing to their low electrical resistance, high active surface area, chemical stability, and electrocatalytic proprieties in many electrochemical reactions. Owing to the excellent combination between high transmittance and high conductivity, CNTs have already been extensively used as electrode materials for spectroelectrochemistry[14] or photovoltaic devices.

Over the last decade there has been a steady increase in the development of new analytical devices that synergically combine nanomaterials with ECL to obtain very low limits of detection and high accuracy even for complex matrices, such as urine or lysate.[15, 2a] There are few examples in literature of CNT electrodes for ECL applications.[16] Rusling demonstrated in

[a] *Dr. G. Valenti, Dr. M. Zangheri, Dr. S. E. Sansaloni, Prof. M. Mirasoli, Prof. A. Roda, Prof. F. Paolucci*
Dipartimento di Chimica "G. Ciamician"
Università di Bologna, via Selmi 2, 40126 Bologna (Italy)
E-mail: g.valenti@unibo.it

[b] *Dr. S. E. Sansaloni, Dr. A. Penicaud*
Centre de Recherche Paul-Pascal CRPP
Avenue A. Schweitzer, 33600, Pessac (France)

[c] *Prof. F. Paolucci*
IENI-CNR Bologna Associate Unit
University of Bologna, via Selmi 2, 40126, Bologna (Italy)

a pioneering work, the highly superior sensitivity of CNTs forest electrodes for prostate cancer detection, electrodes that showed a limit of detection down to 1 pg mL^{-1} in patient serum.[17]

Here, we present the application of optically transparent electrodes based on carbon nanotubes to ECL, demonstrating the electrocatalytic superiority of such materials compared with ITO electrodes and, moreover, for the first time to the best of our knowledge, the ideal suitability of nanotubes as electrode material for developing new devices for ECL imaging of cells and tissues.

Results and Discussion

Our platform consists of a CNT electrode film deposited directly on glass, on polyethylene terephthalate (PET) or any support that resists NaOH (1 M). To enhance the conductivity and the electrochemical properties, the electrodes were made with a dissolution methodology that guarantees the preservation of the electronic properties of pristine CNTs.[18] In brief, the CNTs were dissolved by reducing them in an aprotic environment, then the solution was filtered onto alumina and transferred directly onto the holder (for more details see Experimental Section). The electrodes obtained with this procedure show versatile electric and transmission properties that can be modified, in theory at will, by changing the amount of CNT solution used in the preparation.[19]

In this case, we used optically transparent electrodes with a typical conductivity of 1100 Ω sq^{-1} and a transmittance higher than 90% (the material properties were fully characterized with different experimental techniques, namely AFM, SEM, Raman spectroscopy, see Figure 1 and Figures S1–S3 in the Supporting Information). The electrochemical responses of the CNT electrodes were tested by using a redox mediator, that is, ferrocyanide ($[Fe(CN)_6]^{4-}$). A typical cyclic voltammogram (CV), reported in Figure 2, shows the reversible oxidation of ferrocyanide in phosphate buffer solutions. The CNT electrode shows good electrochemical behavior, with a peak-to-peak separation of 60 mV even at a high scan rate (1 Vs^{-1}).

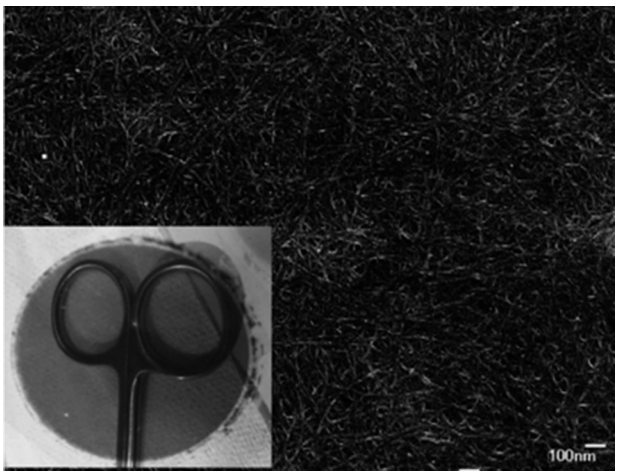

Figure 1. Scanning electron microscopy image of the CNT electrode. Inset: photograph of the transferred CNT electrodes on polyethylene terephthalate (PET) substrate.

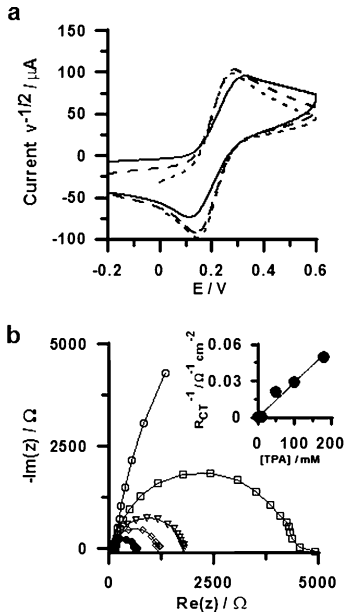

Figure 2. a) Cyclic voltammogram of the CNT-based electrode in 1 mM $[Fe(CN)_6]^{4-}$/$LiClO_4$ 0.1 M aqueous solution. Scan rate = 1 (solid curve), 0.2 (dashed curve), 0.1 Vs^{-1} (dotted curve). b) Impedance spectroscopy (ESI–Nyquist plot) for different TPrA concentrations: 1 (○), 10 (□), 50 (▽), 100 (◇), 200 mM (●) in phosphate buffer 0.1 M (pH 6.8). Frequencies from 1 MHz to 10 mHz for the fitting details see the Supporting Information. Inset: R_{CT}^{-1} as a function of TPrA concentration. $R_{CT}^{-1} = k_{het}F^2(RT)^{-1}k_a[H^+]^{-1}[TPrA]$, where F is the Faraday constant, R the gas constant, T the temperature, k_a the dissociation constant for TPrA. All the potentials are reported vs. Ag/AgCl (3 M).

It is worth noting that the majority of commercially available transparent electrode materials are based on metal oxides, such as ITO or fluorine-doped tin oxide (FTO), which are not stable at acidic pH. The electrode material that we propose is more stable and can be used in acidic or basic conditions.

In addition to high electrical conductivity, two other key parameters should be considered for an efficient ECL platform: (i) the kinetics of the co-reactant electrochemical reaction and (ii) side reactions due to the electrode surface. The combination of ruthenium polypyridine complexes and amine are, thanks to their good electrochemical stability and photophysical proprieties, well-known and commercially used as ECL labels/co-reactant couple.[20] We tested the homogeneous electrochemically generated luminescence by using this well-known system, specifically, $[Ru(bpy)_3]^{2+}$ (bpy = bipyridine) and tripropylamine (TPrA) as sacrificial co-reactant.

In this case, also called the "oxidative–reduction" co-reactant strategy, the ECL can be generated with different mechanisms. Here, we focus our attention on the mechanism that involves only the TPrA oxidation, which is the most important for commercial application (see below).[21] In brief, the direct oxidation of the co-reactant is involved, which partly undergoes a deprotonation reaction, thus forming a highly stably reducing radical species that reduces the ECL luminophore ($[Ru(bpy)_3]^{2+}$) to $[Ru(bpy)_3]^{+}$. On the other hand, the oxidized co-reactant is

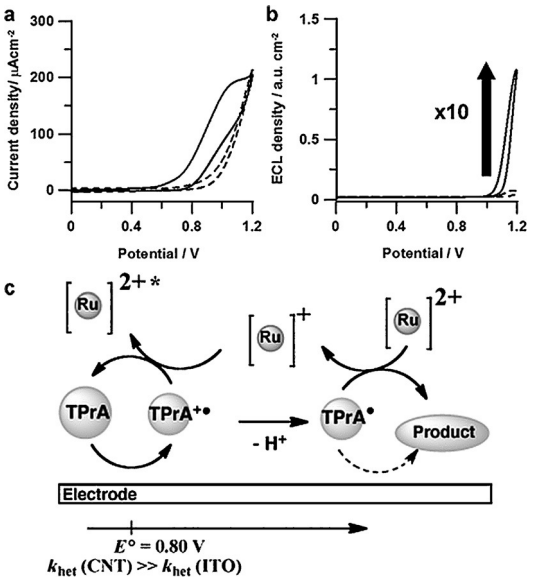

Figure 3. a) Cyclic voltammogram and b) ECL versus potential for 10 mM $[Ru(bpy)_3]^{2+}$, 80 mM TPrA, in phosphate buffer 0.1 M. Solid curves correspond to the CNT-based electrode, whereas dashed curves are for the ITO electrode. Scan rate = 0.1 Vs^{-1}, PMT = 750 V. All potentials are reported vs. Ag/AgCl (3 M). c) Schematic representation for the ECL of $[Ru(bpy)_3]^{2+}$/TPrA. $[Ru]^{2+}$ is $[Ru(bpy)_3]^{2+}$ and $[Ru]^{+}$ is $[Ru(bpy)]^{3+}$.

continuously produced at the electrode surface and thus can react with $[Ru(bpy)_3]^{+}$ and generate the excited state $[Ru(bpy)_3]^{2+}$*, see Figure 3 c.[1] The oxidation of TPrA and the stability of the electrogenerated radicals are the rate-determining steps for the signal generation.[1]

A typical CV, Figure 3 a, and ECL intensity, Figure 3 b, using the CNT electrode (solid curve) as the working electrode in a phosphate buffer solution, with 10 mM $[Ru(bpy)_3]^{2+}$, and 80 mM TPrA is reported in Figure 3. The CV is dominated by a single irreversible oxidation with a potential peak of 1 V (vs. Ag/AgCl) due to the oxidation of TPrA. Interestingly, for commercial ITO under the same experimental conditions, no oxidation of TPrA is observed in that potential region (Figure 3 a, dashed signal).

This different behavior in the CVs prompted us to investigate the kinetics involved at the electrode/solution interface. In particular, we used impedance spectroscopy to estimate the resistance of the charge transfer (R_{CT}) at a fixed potential (@1 V > $E^{\circ}_{TPrA/TPrA+}$) for different TPrA concentrations, which enabled the measurement of the kinetics involved in the TPrA oxidation for the two different electrode materials (see the Supporting Information for details). The oxidation process is 30 times higher for the CNT electrode ($k_{het} = 2.6 \times 10^{-2}$ cm s^{-1}) compared with the commercial ITO ($k_{het} = 8 \times 10^{-4}$ cm s^{-1}). As a consequence of this dramatic difference in the kinetics behavior between the two materials, the ECL emission is more efficiently generated at the CNT electrode. In fact, ECL intensity is ten times higher, at 1.2 V (vs. Ag/AgCl), for the CNT-based electrode compared with ITO; see Figure 3 b. The effective generation of the $[Ru(bpy)_3]^{2+}$ excited state was also confirmed by acquiring the ECL spectrum, which was superimposable with the photoluminescence spectrum, with a maximum emission at 610 nm, which is typical for $[Ru(bpy)_3]^{2+}$* (Figure S5 in the Supporting Information).[22] Here, we normalized the current and ECL signal in Figure 3 for the electroactive surface area. In fact, CNTs are a well-known material with high roughness and high exposed surface area. In general, an increase in the electroactive area leads to an increase in the electrogenerated radical co-reactant and thus an increase in the ECL intensity. The electroactive area for the CNT electrode is three times higher than commercial ITO (see the Supporting Information).

In addition, for the electrochemical generation of the excited state, both the radical cation ($TPrA^{+\bullet}$) and radical ($TPrA^{\bullet}$) should be present at the same time in the diffusion layer. The generation of the radical at an adequate distance from the electrode surface is an important aspect in order to avoid radical oxidation on the electrode, also called oxidative consumption (as shown by the dashed line in Figure 3 c). For this reason, the kinetics involved in the chemical reaction that follows the TPrA oxidation is another key parameter for efficient ECL generation. It was previously reported that oxygen-containing surface species reduced the $TPrA^{+\bullet}$ lifetime, and thus the $TPrA^{\bullet}$ would be subject to more oxidative consumption subsequently, leading to weaker ECL signals.[23] The strategy that we adopted for electrode preparation minimized the oxygen content and defects in the CNTs, thus increasing the conductivity of the electrode and also minimizing the oxidative consumption of the co-reactant (see Raman spectrum in the Supporting Information).

Although many mechanisms for ECL generation have been reported in the literature, the most important for commercial sensors applications, for example, sandwich immunoassays biosensors, is based on the so-called heterogeneous ECL.[24] This strategy consists of a capture site, specific for the analyte, and a detection site with the ECL active dye in proximity to the working electrode, and typically those are two antibodies in a sandwich assembly. In this case, the mechanism for the signal generation is prevalently due to the co-reactant oxidation, similar to the homogeneous case previously described, but with the luminophore constricted in the diffusion layer.[25] In fact, the alternative pathway through the parallel oxidation of TPrA and $[Ru(bpy)_3]^{2+}$ is very unlikely because of the large distance of the latter to the electrode surface, as predicted by Marcus theory.

Our research groups recently reported the first application of heterogeneous ECL for imaging using a new device based on ITO as an optically transparent electrode.[26] This paper opened the frontiers to other ECL applications related to the advanced imaging with high spatial resolution, especially for cell imaging.[27] In this context, we designed an electrochemical cell comprising three electrodes composed of the CNT film assembled on a microscope slide. The electrodes were deposited directly onto the microscope slide with a scotch tape mask used for isolating the three electrodes. The device is schematized in Figure 4 a and b and was applied as a platform for ECL microscopy. For this application we optimized the transmittance of the electrode by choosing as starting materials double-walled CNTs with particularly long length (10 μm) that

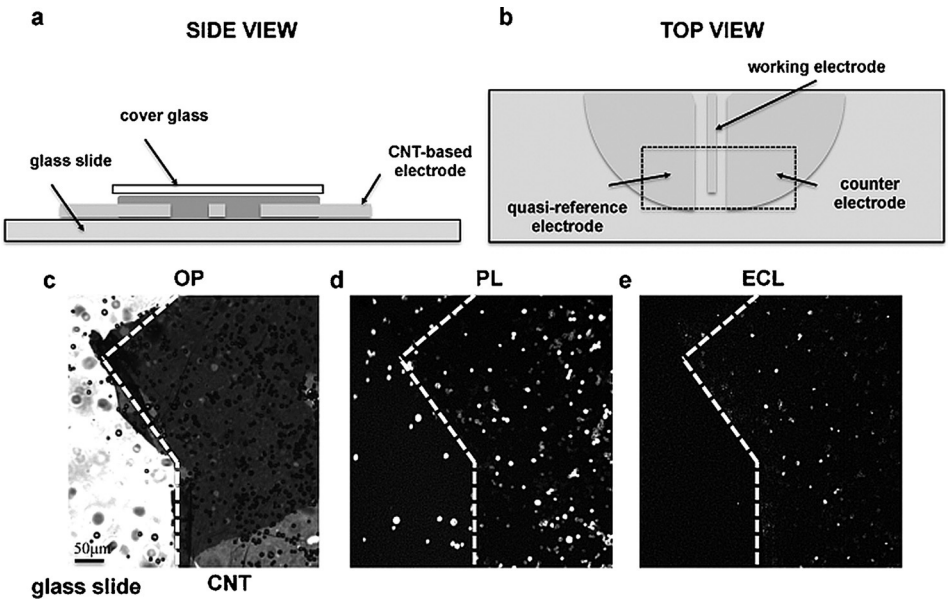

Figure 4. Schematic representation of the CNT-based ECL imaging cell. a) Side view and b) top view. Glass slide 75×25×1 mm. 20× objective/30 ms. c) Optical image, d) photoluminescence image, e) ECL image of the $[Ru(bpy)_3]^{2+}$ labelled microspheres. The white dashed line is a guide for eye to show the electrode/support border.

generate a CNT network with excellent optoelectrical performance (100 $\Omega\,sq^{-1}$ sheet resistance at 90% transmittance in the visible region). These properties open up the application of this electrochemical cell for visualizing biological samples, for example cells, by using inverted microscopy. To mimic a single cell in ECL imaging experiments, we used carboxyl polystyrene microbeads, with dimensions comparable to the size of a cell sample (8 μm), covalently coupled with a specific capture site (aminoderivate of biotin) and ruthenium amino derivate functionalized with streptavidin (see scheme below and the Experimental Section).

After the functionalization, the beads were deposited on the electrode slide in a phosphate buffer solution with 80 mM of TPrA. The optical image obtained with transmittance light is reported in Figure 4c and shows the edge of the working CNT-based electrode. As proof of the successful bioconjugation and of the emission behavior of the modified microbeads, we recorded the fluorescence image reported in Figure 4d. This image was also used for focusing the objective on the beads. Finally, by switching off the light source and applying a positive potential (1.2 V), we recorded the ECL emission, see Figure 4e. The ECL image shows good overlap with the optical one, see Figure 4c and e.

Notice that the emission in the ECL image comes only from the beads on the working electrode surfaces and not from those on the unmodified glass slide. This demonstrated that the emitting light is triggered by the device.

Finally, we compared the performance for the heterogeneous ECL to the two transparent electrode materials (CNTs vs. ITO). The two ECL intensity profiles across a single bead, Figure 5, show an impressive increase in the signal intensity for the CNT-based platform. In line with the aforementioned increase in the intensity for the homogeneous ECL, our transparent platform, which shows catalytic behavior for co-reactant oxidation, is far superior to the commercial ITO, especially for heterogeneous ECL.

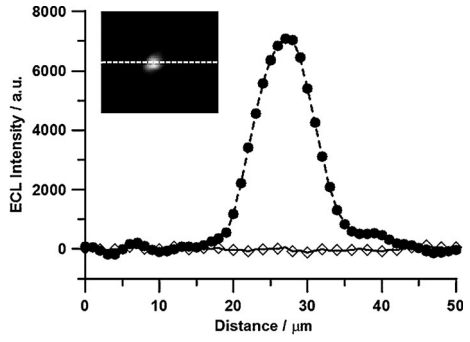

Figure 5. Single-bead ECL intensity profile of a $[Ru(bpy)_3]^{2+}$ labelled microsphere for the CNT (●) or ITO (◇) electrodes in phosphate buffer 0.1 M/ 80 mM TPrA. Potential applied = 1.2 V (vs. Ag/AgCl, 3 M) for 7 s with 20× objective.

Conclusion

We have demonstrated that carbon-based, and in particular carbon nanotube, electrodes are excellent materials for ECL applications thanks to the overpotential of the oxidation of amine derivatives, which are the most commonly used co-reactants for commercially available instruments. By using CNTs we were able to combine transparency with good conductivity. Finally, we demonstrated as proof of principle that our CNT device can be used for ECL imaging in which microbeads were used to mimic a real biological sample for single-cell visualization.

Experimental Section

All the reagents were used without any purification. Tris(2,2′-bipyridine) ruthenium(II) perchlorate, ($[Ru(bpy)_3]^{2+}$), tripropylamine (TPrA), *N*-(3-dimethylaminopropyl)-*N*′-ethyl-carbodiimide hydrochloride (EDC), 3-sulfo-*N*-hydroxysuccinimide (s-NHS), *N*,*N*′-dicyclohexylcarbodiimide (DDC), ferrocyanide $[Fe(CN)_6]^{4-}$ were purchased from Sigma–Aldrich. Bis(2,2′-bipyridine)-[4-(4′-methyl-2,2′-bipyridin-4-yl)butanoic acid] ruthenium bis(hexafluorophosphate) ($Ru(bpy)_3^{2+}$–COOH), and biotin-cadaverine-TFAc were purchased

from Cyanagen (Bologna, Italy). ITO was purchased from Kuramoto Seisakusho Co. Ltd. (Tokyo, Japan). The polystyrene carboxylated microbeads (diameter 8 μm) were purchased from Spherotech (Libertyville, Illinois).

CNT electrode synthesis

The CNT-based electrodes were synthesized and deposited on the support as previously described in the literature (see the Supporting Information and Figure 1).[24] The CNTs were dissolved by reducing them with naphthalene salt in dry THF upon intercalation with metallic potassium in the glovebox. This solution was then filtered onto alumina, which was placed in a hermetically sealed box and transferred outside the glovebox to be placed under a controlled flow of dry air for 2 h at least, in order to reoxidize (neutralization) the film. After that, the alumina membrane with the CNT film was immersed in a sodium hydroxide (1.5 M) bath to dissolve the alumina. The bath was then neutralized with deionized water until pH ≈ 7 was reached. Finally, the electrode support, either a microscope slide or polyethylene terephthalate (PET) foil, was placed at the bottom of the bath and the CNT films were deposited on it by removal of the solvent. The electrodes were dried in the oven overnight at 40–50 °C. Either single-walled carbon nanotubes from CoMoCAT (South West Nano Technologies SWeNT) or double-walled carbon nanotubes from Rice University[28] were used for the electrode preparation. The obtained electrodes were characterized by scanning electron microscopy (SEM), Raman spectroscopy and atomic force microscopy (AFM) (see the Supporting Information for details).

Electrochemical characterization

Cyclic voltammetry (CV), electrochemical impedance spectroscopy (EIS), and chronoamperometry investigations were carried out with a Biologic SP300 potentiostat using a custom-made electrochemical cell described in a previous paper.[29] The working electrode consisted of CNT film or ITO with a constant geometrical area 2 cm in diameter, whereas the counter electrode was a platinum spiral and the reference electrode was homemade Ag/AgCl (3 M).

Electrochemiluminescence detection

The ECL measurements were carried out in a phosphate buffered solution (PBS) using 80 mM TPrA as a sacrificial co-reactant. The counter electrode was a platinum spiral and the reference electrode was homemade Ag/AgCl (3 M). The ECL signal generated by performing the potential step program was measured with a photomultiplier tube (PMT, Hamamatsu R4220p) placed at a constant distance under the cell and inside a dark box. A voltage in the range 550–750 V was supplied to the PMT. The light/current/voltage curves were recorded by collecting the preamplified PMT output signal (by an ultralow-noise Acton research model 181) with the second input channel of the ADC module of the AUTOLAB instrument.

Imaging instrumentation

The CNT imaging platforms has been designed, as described in the Supporting Information, directly onto conventional microscopy slides (7.5 × 2.5 cm). For the ECL imaging the best performances were obtained with a three-electrode configuration: an Ag quasi-reference electrode (25 mm^2), a CNT-based working electrode (8 mm^2), and a CNT-based counter electrode (25 mm^2) with 50 μL of PBS/TPrA solution. For microscopy imaging, an epifluorescence microscope from Nikon (Chiyoda, Tokyo, Japan) equipped with ultrasensitive electron-multiplying CCD camera (EM-CCD 9100–13 from Hamamatsu, Hamamatsu Japan) was used with a resolution of 512 pixel × 512 pixel with a size of 16 × 16 μm. The microscope was enclosed in a homemade dark box to avoid interference from ambient light and was equipped with a motorized microscope stage (Corvus, Marzhauser, Wetzlar, Germany) for sample positioning. The microscope was equipped with long distance objective from Nikon (10×/0.30 DL17, 5 mm, 20×/0.40 DL13 mm, 50×). The integrated system also included a potentiostat from AUTOLAB, suitable for providing the needed potential for the ECL-triggered reaction.

Preparation of $[Ru(bpy)_3]^{2+}$ labelled microspheres

Bis(2,2′-bipyridine)-[4-(4′-methyl-2,2′-bipyridin-4-yl)butanoic acid] ruthenium bis(hexafluorophosphate) ($Ru(bpy)_3^{2+}$–COOH) was conjugated to streptavidin (Scheme 1) according to the following protocol: A volume of 70 μL of $Ru(bpy)_3^{2+}$–COOH (7.1×10^{-3} M in DMF) was added to 1.5 equivalents of *N*,*N*′-dicyclohexylcarbodiimide (DDC) and the reaction solution was gently mixed for 4 h at room temperature (25 °C). A streptavidin solution (630 μL of 2.0×10^{-5} M) in 0.1 M borate buffer (pH 9.4) was then added to conjugate streptavidin to the activated $Ru(bpy)_3^{2+}$–COOH. The solution was incubated overnight and the labelled protein was subsequently purified with dialysis against 5 L of PBS. Beads were then conjugated to the amino derivative of biotin (Scheme 1). The suspension of beads (200 μL) was washed three times in 0.1 mol L^{-1} borate buffer

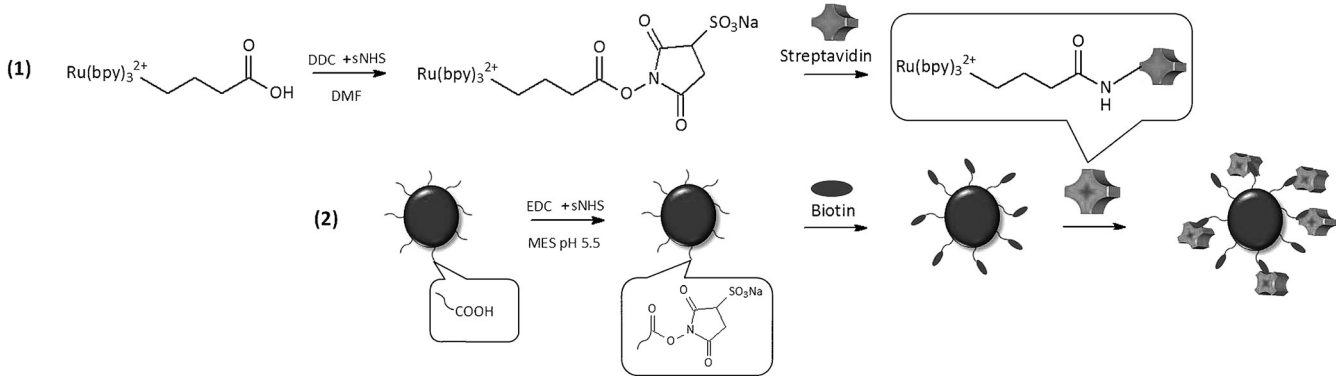

Scheme 1. Ru@μbeads functionalization for heterogeneous ECL. Schematic representation for 1) $Ru(bpy)_3^{2+}$–COOH conjugation with streptavidin and 2) for the synthesis of labelled carboxyl polystyrene microbeads (Ru@μbeads).

(pH 9.6) and two times in 0.1 mol L^{-1} in 2-(*N*-morpholino)ethanesulfonic acid buffer (MES pH 5.5). Upon resuspending the beads in 250 μL of MES buffer, *N*-(3-dimethylaminopropyl)-*N'*-ethyl-carbodiimide hydrochloride (EDC) and s-NHS were added to a final concentration of 50 mM and 2 mM, respectively. The reaction mixture was mixed for 1 h at RT. After a washing cycle (as described above), 500 μL of 9 mM biotin cadaverine in 0.1 mol L^{-1} borate buffer (pH 8.6) was added. The mixture was incubated overnight at 4 °C, and the solution was finally washed three times in PBS. Beads conjugated to biotin were then coupled with the streptavidin–$Ru(bpy)_3^{2+}$ using the following procedure. A suspension of 50 μL of beads was centrifuged and after buffer removal, 50 μL of labelled streptavidin was added. The mixture was gently mixed for 2 h at RT and then three washing steps were performed by centrifugation and resuspension with PBS.

Acknowledgements

We thank the University of Bologna Italian Ministero dell'Istruzione, Università e Ricerca (MIUR-project PRIN 2012 and FARB-2014), Fondazione Cassa di Risparmio in Bologna, and the FIRB project "NANOSOLAR''. The authors gratefully acknowledge Prof. Matteo Pasquali and Dr Francesca Mirri from Rice University (Houston, Texas) for the double-walled carbon nanotubes. A.P., G.V., and F.P. thank the Agence Nationale de la Recherche (GRAAL) and the Aquitaine region for a grant to support collaboration with the Emilia Romagna region. S.E. thanks the project Bio-orthogonal chemo-specific ligation (BIOCHEMLIG-Project: 238434) funded under 7th Framework Programme for financial support.

Keywords: chemiluminescence · electrochemistry · imaging · nanotubes · transparent electrodes

[1] a) A. J. Bard, in *Electrogenerated Chemiluminescence*, Marcel Dekker, New York, **2004**; b) M. M. Richter, *Chem. Rev.* **2004**, *104*, 3003 – 3036.
[2] a) R. J. Forster, P. Bertoncello, T. E. Keyes, *Annu. Rev. Anal. Chem.* **2009**, *2*, 359; b) L. Z. Hu, G. B. Xu, *Chem. Soc. Rev.* **2010**, *39*, 3275 – 3304.
[3] a) W. Miao, *Chem. Rev.* **2008**, *108*, 2506 – 2553; b) Z. Liu, W. Qi, G. Xu, *Chem. Soc. Rev.* **2015**, *44*, 3117 – 3142.
[4] a) D. Bruce, J. McCall, M. Richter, *Analyst* **2002**, *127*, 125 – 128; b) S. Workman, M. Richter, *Anal. Chem.* **2000**, *72*, 5556 – 5561.
[5] a) F. Li, Y. Zu, *Anal. Chem.* **2004**, *76*, 1768 – 1772; b) Y. Zu, A. J. Bard, *Anal. Chem.* **2000**, *72*, 3223 – 3232.
[6] a) J. L. Delaney, C. F. Hogan, J. Tian, W. Shen, *Anal. Chem.* **2011**, *83*, 1300 – 1306; b) J. Yan, M. Yan, L. Ge, S. Ge, J. Yu, *Sens. Actuators B* **2014**, *193*, 247 – 254; c) N. Hao, M. Xiong, J. Zhang, J. Xu, H. Chen, *Anal. Chem.* **2013**, *85*, 11715 – 11719.
[7] E. K. Walker, D. A. Vanden Bout, K. J. Stevenson, *Langmuir* **2012**, *28*, 1604 – 1610.
[8] Y. Kim, J. Kim, *Anal. Chem.* **2014**, *86*, 1654 – 1660.
[9] V. Zamolo, G. Valenti, E. Venturelli, O. Chaloin, M. Marcaccio, S. Boscolo, V. Castagnola, S. Sosa, F. Berti, G. Fontanive, M. Poli, A. Tubaro, A. Bianco, F. Paolucci, M. Prato, *ACS Nano* **2012**, *6*, 7989 – 7997.
[10] L. Li, Y. Chen, Q. Lu, J. Ji, Y. Shen, M. Xu, R. Fei, G. Yang, K. Zhang, J.-R. Zhang, J.-J. Zhu, *Sci. Rep.* **2013**, *3*, 1 – 10.
[11] G. Valenti, E. Rampazzo, S. Bonacchi, T. Khajvand, R. Juris, M. Montalti, M. Marcaccio, F. Paolucci, L. Prodi, *Chem. Commun.* **2012**, *48*, 4187 – 4189.
[12] a) S. Deng, J. Lei, Y. Huang, Y. Cheng, H. Ju, *Anal. Chem.* **2013**, *85*, 5390 – 5396; b) Y. Sua, Y. Lv, *RSC Adv.* **2014**, *4*, 29324 – 29339.
[13] a) K. Shao, J. Wang, X. Jiang, F. Shao, T. Li, S. Ye, L. Chen, H. Han, *Anal. Chem.* **2014**, *86*, 5749 – 5757; b) H. Wang, Y. Chai, R. Yuan, Y. Cao, L. Bai, *Anal. Chim. Acta* **2014**, *815*, 16 – 21.
[14] A. Heras, A. Colina, J. López-Palacios, A. Kaskela, A. G. Nasibulin, V. Ruiz, E. I. Kauppinen, *Electrochem. Commun.* **2009**, *11*, 442 – 445.
[15] E. Rampazzo, S. Bonacchi, D. Genovese, R. Juris, M. Marcaccio, M. Montalti, F. Paolucci, M. Sgarzi, G. Valenti, N. Zaccheroni, L. Prodi, *Coord. Chem. Rev.* **2012**, *256*, 1664 – 1681.
[16] a) K. N. Han, C. Ai Li, M.-P. Ngoc Bui, G. H. Seong, *Langmuir* **2010**, *26*, 598 – 602; b) A. Venkatanarayanan, K. Crowley, E. Lestini, T. E. Keyes, J. F. Rusling, R. J. Forster, *Biosens. Bioelectron.* **2012**, *31*, 233 – 239.
[17] N. P. Sardesai, J. C. Barron, J. F. Rusling, *Anal. Chem.* **2011**, *83*, 6698 – 6703.
[18] a) A. Pénicaud, F. Dragin, G. Pécastaings, M. He, E. Anglaret, *Carbon* **2014**, *67*, 360 – 367; b) A. Pénicaud, P. Poulin, A. Derré, E. Anglaret, P. Petit, *J. Am. Chem. Soc.* **2005**, *127*, 8 – 9.
[19] A. Catheline, F. Paolucci, G. Valenti, P. Poulin, A. Pénicaud, *J. Mater. Res.* DOI: 10.1557/jmr.2015.166.
[20] a) E. Kerr, E. H. Doeven, G. J. Barbante, C. F. Hogan, D. J. Bower, P. S. Donnelly, T. U. Connell, P. S. Francis, *Chem. Sci.* **2015**, *6*, 472 – 479; b) L. Della Ciana, S. Zanarini, R. Perciaccante, E. Marzocchi, G. Valenti, *J. Phys. Chem. C* **2010**, *114*, 3653 – 3658; c) Y. Yuan, S. Han, L. Hu, S. Parveen, G. Xu, *Electrochim. Acta* **2012**, *82*, 484 – 492.
[21] W. Miao, J.-P. Choi, A. J. Bard, *J. Am. Chem. Soc.* **2002**, *124*, 14478 – 14485.
[22] M. Montalti, A. Credi, L. Prodi, T. Gandolfi, *Handbook of Photochemistry*, 3rd ed.,Taylor & Francis, Boca Raton, FL, **2006**.
[23] Z. Chen, Y. Zu, *J. Phys. Chem. C* **2008**, *112*, 16663 – 16667.
[24] http://www.roche-diagnostics.co.in/Products/Pages/RocheElecsys Systems.aspx.
[25] M. Sentic, M. Milutinovic, F. Kanoufi, D. Manojlovic, S. Arbault, N. Sojic, *Chem. Sci.* **2014**, *5*, 2568 – 2572.
[26] L. S. Dolci, S. Zanarini, L. Della Ciana, F. Paolucci, A. Roda, *Anal. Chem.* **2009**, *81*, 6234 – 6241.
[27] a) F. Han, H. D. Fang, D. Jiang, *Anal. Chem.* **2014**, *86*, 6896 – 6902; b) M.-S. Wu, D.-J. Yuan, J.-J. Xu, H.-Y. Chen, *Chem. Sci.* **2013**, *4*, 1182 – 1188.
[28] F. Mirri, A. W. K. Ma, T. T. Hsu, N. Behabtu, S. L. Eichmann, C. C. Young, D. E. Tsentalovich, M. Pasquali, *ACS Nano* **2012**, *6*, 9737 – 9744.
[29] G. Valenti, L. Bardini, D. Bonazzi, S. Rapino, M. Marcaccio, F. Paolucci, *J. Phys. Chem. C* **2010**, *114*, 22165 – 22170.